Dynamic Pressurization Method for Measuring Permeability and Modulus: I. Theory

George W. Scherer*

Princeton University, Civil & Env. Eng./PRISM, Eng. Quad. E-319, Princeton, NJ 08544
USA

ABSTRACT

The permeability of a saturated porous body can be determined from the kinetics of dilatation resulting from a change in pressure in the surrounding bath. This method was previously applied to aerogels [J. Gross and G.W. Scherer, J. Non-Cryst. Solids 325 (2003) 34-47]. The theory is here extended to allow for the compressibility of the solid phase, so that the method can be applied to more rigid materials, such as concrete. A viscoelastic analysis indicates that creep of the sample will have a small effect on the measured permeability for cementitious materials, in most cases. However, the effect of entrapped air in the pore liquid is shown to have a drastic effect on the relaxation behavior, so it is essential to reduce the air content below ~0.1 volume %. For samples without entrapped air, a simple result is obtained that is tested in a companion paper.

---

* Author to whom correspondence should be addressed. Email: scherer@princeton.edu

1. Introduction

The permeability of concrete controls the rate at which it absorbs water and saline solutions [1,2], so knowledge of the permeability of concrete is essential for assessing its durability. Unfortunately, conventional methods for measuring permeability are slow (so the sample can change during the course of the experiment [3]) and subject to errors owing to leaks of fluids subjected to high pressure [4]. For materials, such as cement paste and mortar, that are homogeneous on a centimeter scale, the most practical permeability measurement technique is beam-bending [5,6,7,8]. Bending a saturated beam creates a pressure gradient in the pore fluid, which flows until its pressure equilibrates with that in the surrounding bath. The force required to hold the beam at a fixed deflection changes with the pore pressure; since the rate of relaxation of the force depends on the permeability, an analysis of the force yields the permeability (as well as the elastic modulus and stress relaxation function). In principle, the bending method could be applied to concrete, but it would require impractically large samples (viz., minimum cross-section of 10 cm, minimum length/diameter ratio of 10, for a length of > 1 meter and a weight >25 kg). It would be ideal to have a method that uses standard strength cylinders for measuring permeability. Thermopermeametry (TPA) [9] can be used for heterogeneous materials, and has been demonstrated to work for cement paste [10,11,12], as well as gels [13]. The principle is that the pore liquid expands much more than the solid phase when a saturated body is heated, so the expanded liquid tends to flow out of the pores; if the permeability is low, then the thermal strain of the body will show time-dependent effects related to the flow of the pore liquid. This phenomenon is responsible for the well-known overshoot in the expansion of cement and concrete [14,15,16]. Recent attempts to apply the method to mortar, however, have shown that it is difficult to produce samples with the necessary degree of saturation [17,18].

This paper presents an analysis of a method called dynamic pressurization (DP) for measuring permeability by applying hydrostatic pressure on a saturated sample. The principle is illustrated in Figure 1. A saturated sample is equilibrated in a pressure vessel containing a liquid at pressure p_0 (typically, atmospheric). At the start of the measurement (time $t = 0^+$), the pressure in the vessel (p_v) is suddenly increased to $p_v = p_A$ and the sample contracts, exhibiting a linear strain of ε_0. The magnitude of ε_0 depends on the bulk modulus of the porous solid, whose bulk modulus is K_p, and on the bulk modulus of the pore liquid, K_L. Unless $K_p << K_L$ (as is the case for gels), the pore pressure is less than the applied pressure ($p_p < p_A$) immediately after the pressure jump occurs. However, over a period of time that depends on the permeability of the body, liquid from the vessel will flow into the pores and raise p_p to p_A. As the pore pressure increases, the sample will re-expand somewhat, reaching a final strain of ε_∞ that depends on the bulk modulus of the solid phase, K_S. That is, once the pressure has equilibrated in the sample and the vessel, the solid phase is hydrostatically compressed by pressure p_A. By measuring the kinetics of re-expansion, the permeability of the sample can be found; additionally, K_S is obtained from ε_∞, and K_p can be found from ε_0, if K_L is known and Poisson's ratio of the solid is known or can be estimated.

Dynamic pressurization was previously applied to aerogels containing supercritical fluid or vapor [19]. In that case, the solid network was so compliant that K_p was negligible compared to K_S or K_L, which simplifies the analysis considerably. Therefore, in the following section, the kinetics of a DP experiment is examined in detail for the general case, where K_p/K_S is near unity. First, we present an elastic analysis, then examine the importance of viscoelastic relaxation of the solid phase. This was found to be important for TPA [11,12], but will be shown to be less so for DP. A much more important problem is the presence of air bubbles in the pore liquid, because the equilibration of the pore pressure is dramatically delayed while the bubbles are being compressed. When bubbles are present, the kinetics cannot be calculated analytically, but we present numerical solutions to illustrate the magnitude of the problem. An experimental study [20] indicates that the kinetics of relaxation are well described by the elastic analysis, as long as the sample is saturated, but that long times can be required to achieve the required degree of saturation.

2. Theory

The analysis of the DP experiment is based on the theory developed by Biot [21] and discussed in detail by Coussy [22]. The application of the theory to problems of the present type has recently been reviewed [23], so in this section we simply present the constitutive and continuity equations without derivation. The elastic case is presented in section 2.1 and the viscoelastic case in 2.2, for samples whose pores are saturated with liquid. When pockets of air or vapor are present in the pores, a different approach is required, as explained in section 2.3.

2.1. Saturated elastic materials

For a saturated porous body whose solid phase is elastic, the form of the constitutive equation is

$$\varepsilon_z = \varepsilon_f + \frac{1}{E_p}\left[\sigma_z - \nu_p\left(\sigma_r + \sigma_\theta\right)\right] \tag{1}$$

where ε_z is the axial strain, $\sigma_r, \sigma_\theta, \sigma_z$ are the total stresses in the principal directions, and E_p and ν_p are Young's modulus and Poisson's ratio for the drained porous solid. The free strain is defined by

$$\varepsilon_f = \frac{bp}{3K_p} \tag{2}$$

where p is the pore pressure, the bulk modulus of the drained porous solid is $K_p = E_p/[3(1\text{-}2\nu_p)]$, and the Biot coefficient is

$$b = 1 - \frac{K_p}{K_S} \tag{3}$$

where K_S is the bulk modulus of the solid phase. Transport of the pore fluid is assumed to obey Darcy's law [24], which means that the flux (J) of fluid is proportional to the gradient in pressure:

$$J = -\frac{k}{\eta_L}\nabla p \tag{4}$$

where k is the permeability (with units of area) and η_L is the viscosity of the liquid. The continuity equation is

$$\frac{\dot{p}}{M} + b\dot{\varepsilon} = \frac{k}{\eta_L}\nabla^2 p \tag{5}$$

where ε is the volumetric strain and the superscript dot indicates a partial derivative with respect to time. The Biot modulus, M, is defined by

$$\frac{1}{M} = \frac{\phi}{K_L} + \frac{b - \phi}{K_S} \tag{6}$$

where ϕ is the (liquid-filled) porosity and K_L is the bulk modulus of the pore liquid (or, the reciprocal of its compressibility).

We are interested in a cylindrical sample with radius R, in which the flow is entirely in the radial direction. In that case, eq. (5) becomes

$$\frac{\dot{p}}{M}+b\dot{\varepsilon}=\frac{k}{\eta_L R^2}\frac{1}{u}\frac{\partial}{\partial u}\left(u\frac{\partial p}{\partial u}\right) \tag{7}$$

where $u = r/R$ is the dimensionless radial coordinate. For a saturated cylindrical body surrounded by fluid at pressure p_A, the volumetric strain is [19]

$$\varepsilon = 3\beta\varepsilon_f + 3(1-\beta)\langle\varepsilon_f\rangle - \frac{p_A}{3K_p} \tag{8}$$

where the angle brackets indicate a volumetric average, such that

$$\langle y\rangle \equiv \frac{2}{R^2}\int_0^R y(r)r\,dr = 2\int_0^1 y(u)u\,du \tag{9}$$

The constant β is defined by

$$\beta=\frac{1+\nu_p}{3(1-\nu_p)} \tag{10}$$

Using eqs. (2), (7), and (8), we obtain a partial differential equation for the pore pressure that can be written in the following form:

$$\frac{\partial p}{\partial\theta}+\left(\frac{(1-\beta)b\lambda}{1-(1-\beta)b\lambda}\right)\frac{\partial\langle p\rangle}{\partial\theta}-\left(\frac{\lambda}{1-(1-\beta)b\lambda}\right)\frac{\partial p_A}{\partial\theta}=\frac{1}{u}\frac{\partial}{\partial u}\left(u\frac{\partial p}{\partial u}\right) \tag{11}$$

where

$$\lambda=\frac{Mb}{K_p+Mb^2} \tag{12}$$

The physical significance of λ will be shown in section 2.1.2. The dimensionless time, θ, is defined by

$$\theta=\frac{t}{\tau_v} \tag{13}$$

where the hydrodynamic relaxation time, τ_v, is

$$\tau_v=\frac{\eta_L R^2}{k}\left(\frac{\beta b^2}{K_p}+\frac{1}{M}\right) \tag{14}$$

This is the characteristic time that controls the rate of equilibration of the pore pressure.

We need to solve eq. (11) for $p(u,\theta)$, subject to the following conditions. Initially, the pore pressure is uniform and equal to atmospheric pressure, so $p(u,0) = p_0$; thereafter, the surface is subjected to the applied pressure p_A, so $p(1, \theta) = p_A(\theta)$. The solution is readily obtained by use of the Laplace transform, as shown in Appendix 1. The quantity of interest is the axial strain of the sample, which is found by substituting eq. (25) of ref. 25 into eq. (1):

$$\varepsilon_z = \frac{b\langle p(\theta)\rangle - p_A}{3K_p} \tag{15}$$

Using the average pressure from Appendix 1, the strain is found to be

$$\varepsilon_z = \left(\frac{b-1}{3K_p}\right) p_A(\theta) - \frac{b(1-\lambda)}{3K_p} \int_o^\theta \Omega(\theta-\theta') \frac{dp_A}{d\theta'}\, d\theta' \tag{16}$$

The Laplace transform of the relaxation function, Ω, cannot be inverted analytically, but it can be obtained numerically, as described in Appendix 2. It is approximated with an absolute error < 0.002 by

$$\Omega(\theta) \approx \exp\left\{\frac{4}{\sqrt{\pi}}\left[1-(1-\beta)b\lambda\right]\left(\frac{\theta^{2.2}-\theta^{0.5}}{1-\theta^c}\right)\right\} \tag{17}$$

where the exponent c is

$$c = 0.6 - 0.19(1-\beta)b\lambda \tag{18}$$

The quality of the approximation is shown in Figure 2. The form of the constant term in eq. (17) is chosen to reproduce the exact value of Ω in the limit as $\theta \to 0$:

$$\Omega(\theta) \approx 1 - \frac{4}{\sqrt{\pi}}\left[1-(1-\beta)b\lambda\right]\sqrt{\theta} \tag{19}$$

Thus, $\Omega(0) = 1$ and $\Omega \to 0$ as $\theta \to \infty$; in fact, as shown in Figure 2, relaxation is nearly complete when $\theta \geq 1$.

2.1.1. Step-change in pressure

The most convenient way to do the experiment is to impose an "instantaneous" change in pressure, which means that p_A rises from p_0 to its final value over a period of time that is much less than τ_v. From Figure 2 we see that Ω has relaxed to 0.98 by the time that θ reaches 10^{-4}, so the period during which the pressure change occurs should be $\leq 10^{-4}\ \tau_v$ to avoid significant errors. If that is not possible, then the strain data can be analyzed using eq. (16), taking account of the actual pressure history. In the case where p_A makes a step change at $\theta = 0$, eq. (16) reduces to

$$\varepsilon_z = \varepsilon_\infty + \left(\varepsilon_0 - \varepsilon_\infty\right)\Omega(\theta) \tag{20}$$

where the instantaneous strain is

$$\varepsilon_0 = -\left(1 - b\lambda\right)\frac{p_A}{3K_p} \tag{21}$$

and the final strain is

$$\varepsilon_\infty = -\frac{p_A}{3K_S} \tag{22}$$

From eqs. (15) and (20), we find that the average pressure in the sample at the moment that the pressure jump occurs is

$$\left\langle p(0)\right\rangle = \lambda p_A \tag{23}$$

Thus, the parameter λ, defined in eq. (12), represents the ratio of the pore pressure to the applied pressure following a sudden pressure jump. In the gel limit ($K_p << K_L$, K_S), $\lambda = 1$, so eq. (23) indicates that the pore pressure is immediately equilibrated with the applied pressure, because the liquid is not sheltered when the solid network is extremely compliant. The initial strain, eq. (21) then depends only on the compressibilities of the individual phases:

$$\varepsilon_0 \approx -\frac{p_A}{3M} \approx -\frac{p_A}{3}\left(\frac{\phi}{K_L} + \frac{1-\phi}{K_S}\right)\ ,\ K_p << K_L, K_S \tag{24}$$

where M is the Biot modulus, defined in eq. (6), in the gel limit where $b = 1$. On the other hand, if the pore liquid is compliant (for example, if the pores contain vapor), then

$K_L << K_p$, K_S; in that case, λ reduces to

$$\lambda \approx \frac{b}{\phi}\frac{K_L}{K_p} << 1 \ \ , \ K_L << K_p, K_S \tag{25}$$

Then eq. (21) reduces to

$$\varepsilon_0 \approx -\frac{p_A}{3K_p} \ \ , \ K_L << K_p, K_S \tag{26}$$

which means that the initial deformation is controlled only by the rigidity of the porous solid network, when no reinforcement is offered by the liquid.

2.1.2. Step depressurization

Suppose that a step increase in pressure is applied at $\theta = 0$, and then the pressure is reduced suddenly to zero at $\theta = \theta_d$. In this case, eq. (16) leads to

$$\varepsilon_z = \begin{cases} \varepsilon_\infty + (\varepsilon_0 - \varepsilon_\infty)\,\Omega(\theta) & , 0 \le \theta \le \theta_d \\ (\varepsilon_0 - \varepsilon_\infty)\left[\Omega(\theta) - \Omega(\theta - \theta_d)\right] & , \ \theta \ge \theta_d \end{cases} \tag{27}$$

The form of the strain is illustrated in Figure 3. If θ_d is late enough so that $\Omega(\theta)$ has effectively relaxed to zero, then the strain following depressurization is simply given by

$$\varepsilon_z = (\varepsilon_\infty - \varepsilon_0)\,\Omega(\theta - \theta_d), \ \ \theta \ge \theta_d \tag{28}$$

In this case, the shape of the relaxation curve is the same in the pressurization and depressurization steps, so the same information is obtained in both steps. If the curves are not identical, it is an indication of a problem with the experiment, such as the existence of trapped air in the pores. This is discussed further in section 2.3.

2.1.3. Extracting parameters from the data

From eq. (22) we see that the bulk modulus of the solid phase is found directly from the final strain value:

$$K_S = -\frac{p_A}{3\varepsilon_\infty} \tag{29}$$

If we let x be the ratio of the initial and final strains,

$$x = \frac{\varepsilon_0}{\varepsilon_\infty} = \frac{1 - b\lambda}{1 - b} \tag{30}$$

then the bulk modulus of the porous network can be found from eqs. (21) and (22):

$$K_p = K_S \left[\frac{\phi - (x + \phi - 1) K_L / K_S}{x\phi - (x\phi + x - 1) K_L / K_S} \right] \tag{31}$$

Generally, $K_L / K_S << 1$ (for example, $K_L = 2.2$ GPa [26] for water and $K_S \approx 30$ GPa [6]), so eq. (31) reduces to

$$K_p \approx \frac{K_S}{x} \approx -\frac{p_A}{3\varepsilon_0} \tag{32}$$

so

$$b \approx 1 - \frac{1}{x} \tag{33}$$

Eq. (32) is a relatively crude approximation, as it implies that $\lambda = 0$, whereas a typical value for a cementitious material would be $\lambda \approx 0.2$-0.3; however, rough approximations to the moduli are sufficient for calculating the permeability, k. To find k, the data for strain versus time must be fitted to eqs. (17) and (20) to extract τ_v as a fitting parameter. The permeability is then given by

$$k = \frac{\eta_L R^2}{\tau_v} \left(\frac{\beta b^2}{K_p} + \frac{1}{M} \right) \tag{34}$$

To evaluate eq. (34), a measurement or estimate of β is required; for cementitious materials, $\nu_p \approx 0.2$ [27], so $\beta \approx 0.5$. Except for gels, K_L is usually much smaller than K_p or K_S, so the latter values do not need to be known very accurately to get a good value for k; only K_L and ϕ are important, as they control the value of M, while the terms involving K_p and K_S are relatively small.

2.2. Stress in the porous elastic body

During pressurization, the body is compressed and there is little risk of damage. However, during depressurization the tensile stress in the porous solid may exceed the tensile strength if the pressure in the chamber drops too rapidly. In this subsection, we will calculate the stresses generated during a step change and a linear change in pressure.

From eq. (25) of ref. 25, the axial stress in the body is found to be

$$\sigma_z(r) = -p_{ext} + \left(\frac{E_p}{1-\nu_p}\right)\left(\langle\varepsilon_f\rangle - \varepsilon_f\right) = -p_{ext} + \left(\frac{1-2\nu_p}{1-\nu_p}\right) b\left(\langle p\rangle - p\right) \tag{35}$$

Here we have written p_{ext} for the pressure at the exterior surface of the sample. As explained in ref. 25, the stress that contributes to opening cracks is not σ_z, but $\sigma_z + p_{ext}$. This is so, because the external pressure acts within the crack to push it open, thus compensating the effect of the pressure on the ends of the sample which tends to push flaws shut. The crack-opening stress in the body can thus be written as

$$\sigma_z^{CO} \equiv \sigma_z + p_{ext} = \left(\frac{1-2\nu_p}{1-\nu_p}\right) b\left(\langle p\rangle - p\right) \tag{36}$$

and the crack-opening stress at the surface is

$$\sigma_z^{CO}(R) = \left(\frac{1-2\nu_p}{1-\nu_p}\right) b\left(\langle p\rangle - p_{ext}\right) = \left(\frac{1-2\nu_p}{1-\nu_p}\right)\left[3K_p\varepsilon_z + (1-b)p_{ext}\right] \tag{37}$$

Suppose that the sample has been exposed to a pressure $p_{ext} = p_A$ until the strain is fully relaxed, and then the pressure is suddenly reduced to zero, as proposed in section 2.1.2. According to eq. (28), the strain at $\theta = \theta_d$ is

$$\varepsilon_z = \varepsilon_\infty - \varepsilon_0 = \frac{b(1-\lambda)p_A}{3K_p}, \quad \theta \ge \theta_d \tag{38}$$

Since $p_{ext} = 0$, eq. (37) indicates that the stress in the body following the pressure drop is

$$\sigma_z^{step} \equiv \sigma_z^{CO}(R) = \left(\frac{1-2\nu_p}{1-\nu_p}\right) b\,(1-\lambda)\,p_A \tag{39}$$

For a cementitious body it is reasonable to assume $\nu_p \approx 0.2$, $b \approx 2/3$, and $\lambda \approx$ ¼, so eq. (39) indicates that the stress resulting from the pressure jump is ~(3/8) p_A; consequently, damage is likely if the pressure step is more than about twice the tensile strength of the sample.

If the strains produced pressure jumps smaller than this are too small, then a large compressive jump can be applied to produce an easily measurable strain, and the pressure can be reduced gradually to avoid damage to the sample. Suppose that the pressure is reduced linearly according to

$$p_{ext} = \begin{cases} p_A & ,0 \le \theta \le \theta_d \\ p_A\left[1 - \dfrac{\theta-\theta_d}{\theta_0}\right] & ,\theta_d \le \theta \le \theta_d + \theta_0 \\ 0 & ,\theta_d + \theta_0 \le \theta \end{cases} \tag{40}$$

where depressurization occurs linearly over the time interval t_0 and we define $\theta_0 = t_0/\tau_v$. This can be written much more compactly as

$$p_{ext} = p_A\left[1 - \left(\frac{\theta-\theta_d}{\theta_0}\right)H(\theta-\theta_d) + \left(\frac{\theta-\theta_d-\theta_0}{\theta_0}\right)H(\theta-\theta_d-\theta_0)\right] \tag{41}$$

where $H(x)$ is the Heaviside function, which is zero when $x < 0$ and unity when $x > 0$. As shown in Appendix 1, the strain in this case is given by

$$\begin{aligned} 3K_p\,\varepsilon_z &= -(1-b)p_{ext}(\theta) - b(1-\lambda)p_A\,\Omega(\theta) \\ &\quad + \frac{b(1-\lambda)p_A}{\theta_0}\int_0^\theta \Omega(\theta-\theta')\left[H(\theta'-\theta_d) - H(\theta'-\theta_d-\theta_0)\right]d\theta' \end{aligned} \tag{42}$$

When $\theta < \theta_d$, the integral is zero and eq. (42) is equivalent to eq. (20). During depressurization,

$$3K_p\,\varepsilon_z = -(1-b)\,p_{ext}(\theta) - b(1-\lambda)\,p_A\,\Omega(\theta) + \frac{b(1-\lambda)\,p_A}{\theta_0}\int_{\theta_d}^{\theta}\Omega(\theta-\theta')\,d\theta' \tag{43}$$

Substituting this result into eq. (37), and assuming that the initial pressure was held long enough to relax the pore pressure (i.e., so that $\Omega(\theta) \approx 0$ for $\theta > \theta_d$), we obtain

$$\sigma_z^{CO}(R) = \frac{\sigma_z^{step}}{\theta_0}\int_{\theta_d}^{\theta}\Omega(\theta-\theta')\,d\theta' \tag{44}$$

Figure 4 shows that the stress from zero at $\theta = \theta_d$ to a maximum at $\theta = \theta_d + \theta_0$; the peak stress decreases rapidly as the interval allowed for depressurization increases. The variation in peak stress with θ_0 is presented in Figure 5, which shows that the stress decreases by about an order of magnitude if the depressurization is allowed to occur over a period of time equal to the relaxation time, τ_v (so $\theta_0 = 1$).

2.3. Saturated viscoelastic materials

If the porous solid is viscoelastic (VE), then the VE analogy [28] can be applied to analyze the axial strain: the stresses and strains in the constitutive equation, eq. (1), are replaced by their Laplace transforms, and the elastic properties are replaced by the transformed relaxation functions. This procedure is described in detail in refs. 5 and 9. Considerable simplification is achieved by recognizing that the Poisson's ratio of a network is more dependent on its connectivity than on the properties of its elements. For example, it is possible to construct a network with $\nu_p < 0$ from solid struts whose own Poisson's ratio is positive [29]. Therefore, since the strains involved in the present case are small, so that there is no significant change in the geometry of the network, we treat ν_p as a constant.

Another way to arrive at the same conclusion regarding ν_p is to recognize that Poisson's ratio is related to the elastic shear and bulk moduli (G_p and K_p, respectively) by

$$\nu_p = \frac{3K_p - 2G_p}{2\left(3K_p + G_p\right)} \tag{45}$$

By analogy [28], Poisson's ratio for a VE material is given by the same expression, except that the moduli are replaced by their respective Laplace transforms. If the shear and bulk moduli have the same relaxation kinetics, described by the relaxation function $\psi(t)$, then when we replace K_p with $K_p\tilde{\psi}$ and G_p with $G_p\tilde{\psi}$ where the tilde indicates the Laplace transform of the variable with respect to t, and s is the transform parameter [30]. Upon introducing those functions into eq. (45), $\tilde{\psi}$ cancels out and we retrieve a constant ν_p. The rationale for assuming identical relaxation kinetics for the bulk and shear moduli is as follows. Any strain can be expressed in terms of deviatoric and dilatational components (for example, a uniaxial strain is 2/3 shear and 1/3 dilatation). When a strain is imposed on a VE material, the shear strains relax about an order of magnitude faster than the dilatational strains, so the relaxation kinetics can be quite accurately described by treating the bulk modulus as a constant, and allowing only shear strains to relax [see discussion in ref. 28, Ch. 7]. For a porous material, stress relaxation is achieved by bending or extensional deformation of the solid struts constituting the network; as long as the strains are too small to change the microstructure significantly, those local relaxations can be accurately approximated by taking account of the shear components alone. Thus, if the shear relaxation kinetics are described by $\psi(t)$, we can ascribe those kinetics to K_p and G_p, leading to the conclusion that ν_p is constant.

An additional complication arises in the analysis of dynamic pressurization, owing to the importance of the hydrostatic pore pressure. The bulk modulus of the solid, K_S, cannot be treated as a constant, as it was in the analysis of bending [5] or thermal expansion [31], where volumetric relaxation would have a small influence on the property of interest. In the present case, relaxation of K_S will directly affect ε_∞ and will therefore alter the shape of the curve from which the permeability is extracted. For oxide liquids, K_S is found to relax by as much as a factor of 3 or 4, but the characteristic time for relaxation is about an order of magnitude longer than for relaxation of shear strains [ref. 28, Ch. 18]. The form of the viscoelastic bulk modulus of the solid is

$$K_S^{VE}(t) = K_{SR} + (K_S - K_{SR})\,\psi_D(t) \tag{46}$$

where K_S is the instantaneous elastic modulus, K_{SR} is the final (relaxed) value of the bulk modulus, and ψ_D is the dilatational relaxation function. It is convenient to rewrite eq. (46) as

$$K_S^{VE}(t) = K_S\,\psi_S(t) \tag{47}$$

where

$$\psi_S(t) = \mu + (1-\mu)\,\psi_D(t) \tag{48}$$

and $\mu = K_{SR} / K_S$. As noted above, $\mu \approx 0.25$-0.4 for oxide liquids, but it might be lower for layered hydrates, such as those present in cementitious materials. According to the VE analogy, we replace K_S in the elastic equations with $K_S\, s\tilde{\psi}_S$.

The VE constitutive equation has the form,

$$\tilde{\varepsilon}_z = \tilde{\varepsilon}_f + \frac{1}{E_p s\tilde{\psi}}\left[\tilde{\sigma}_z - \nu_p\left(\tilde{\sigma}_r + \tilde{\sigma}_\theta\right)\right] \tag{49}$$

where ψ is the uniaxial stress relaxation function [7,28]. The transform of the axial strain is

$$\tilde{\varepsilon}_z = \frac{s\,\tilde{b}\langle\tilde{p}(s)\rangle - \tilde{p}_A}{3K_p\, s\tilde{\psi}} \tag{50}$$

and

$$\tilde{b} = \frac{1}{s} - \frac{K_p\,\tilde{\psi}}{K_S\, s\tilde{\psi}_S} \tag{51}$$

The transform of the continuity equation is

$$\frac{1}{u}\frac{\partial}{\partial u}\left(u\frac{\partial\tilde{p}}{\partial u}\right) = c_1\,\tilde{p} + c_2 \tag{52}$$

where

$$c_1 = s\,\tau_E\left[\frac{\phi K_p}{\beta K_L} + \frac{\left(s\,\tilde{b} - \phi\right)K_p}{\beta K_S} + \frac{s\,\tilde{b}^2}{\tilde{\psi}}\right] \tag{53}$$

$$c_2 = s\,\tilde{b}\;\tau_E\left[\frac{(1-\beta)s\,\tilde{b}\langle\tilde{p}\rangle - \tilde{p}_A}{\beta\tilde{\psi}}\right] \tag{54}$$

and

$$\tau_E = \frac{\beta\eta_L R^2}{k K_p} \tag{55}$$

The solution for the transform of the axial strain is

$$\tilde{\varepsilon}_z = -\left(\frac{\tilde{p}_A}{3K_p\, s\, \tilde{\psi}}\right)\left\{\frac{c_1\tilde{\psi}\left[1 - s\tilde{b}\, h(c_1)\right] - \tau_E\left(s\tilde{b}\right)^2\left[1 - h(c_1)\right]}{\beta c_1\tilde{\psi} + (1-\beta)\tau_E\left(s\tilde{b}\right)^2\left[1 - h(c_1)\right]}\right\} \tag{56}$$

where

$$h(c_1) = \frac{2I_1\left(\sqrt{c_1}\right)}{\sqrt{c_1}\, I_0\left(\sqrt{c_1}\right)} \tag{57}$$

and I_j is a modified Bessel function of the first kind of order j. The strain is calculated by inverting the transform, given by eq. (56), numerically, as explained in Appendix 2.

To illustrate the effect of VE relaxation, we will present calculations using measured and estimated properties of a Type III Portland cement paste made in our lab with water/cement ratio = 0.45, aged for one month in lime-saturated water [17]: K_L = 2.2 GPa [26], ν_p = 0.2 [27], E_p = 18.5 GPa, K_p = 10.3 GPa, ϕ = 0.48, K_S (estimated) = 38.0 GPa; using these values, we obtain b = 0.73, M = 4.4 GPa, λ = 0.26. The form of the uniaxial relaxation function is taken from ref. 7:

$$\psi(t) = \frac{\exp\left[-\left(t/\tau_2\right)^{0.35}\right]}{1 - \exp\left[-\left(t/\tau_1\right)^{0.18}\right] + \exp\left[-\left(t/\tau_2\right)^{0.35}\right]} \tag{58}$$

This function has been found to provide an excellent fit to stress relaxation data for cement pastes from 1 to 360 days of age [6,7,8] and for mortar [17]. For the present calculations, we use $\tau_1 = 1.7 \times 10^9$ s and $\tau_2 = 1.7 \times 10^4$ s, as measured on the one-month old paste. The average relaxation time, found by integrating eq. (58) over time from 0 to ∞, is $\tau_{VE} = 2.9 \times 10^5$ s; this is relatively short, probably because the experiment was only continued long enough to relax ~20% of the stress, so the long-time tail of ψ was not captured. For this type of paste, longer relaxation runs indicate that τ_{VE} exceeds 10^6 s within 4 days of curing [7], and continues to rise thereafter; in mortar, relaxation is slower the higher the sand content [17]. To evaluate the influence of VE relaxation, we will evaluate eq. (56) for various values of the ratio

$$\Lambda = \frac{\tau_v}{\tau_{VE}} \tag{59}$$

which is a measure of the relative rates of hydrodynamic relaxation (of the pore pressure) and stress relaxation in the porous network. Since we have no information about the kinetics of dilatational relaxation of the solid phase, we will use eq. (58) to represent ψ_D in eq. (48). Since dilatational relaxation is expected to be much slower than uniaxial relaxation of the network, this choice exaggerates the importance of viscoelasticity. We can also evaluate the relative importance of shear and dilatational relaxation by the choice of μ: if $\mu = 1$, then the solid phase does not relax; a more realistic choice (based on the behavior of oxide melts) is $\mu \approx 0.3$.

Figure 6 shows the normalized strain for several values of Λ when $\mu = 1$ or 0.3. In the former case, the curves have the same appearance, so the experimentalist has no indication that relaxation is occurring. Application of eq. (29) would yield an underestimate of K_S. Fortunately, since the shape of the curves barely changes, the value of k obtained by fitting to eq. (20) would be fairly accurate, as shown in Figure 7. The value of τ_v extracted from the fit agrees within ≤ 20%, as long as $\Lambda \leq 0.1$. Since τ_{VE} is typically > 10^6 s, this indicates that the permeability could be obtained with an error no greater than 20%, as long as the hydrodynamic relaxation time is ≤ 10^5 s. Recent DP experiments performed on a cement paste with a permeability of ~10^{-21} m^2 had a relaxation time of ~10^5 s for a sample with R= 4.9 cm. Therefore, we expect modest errors even for very low permeabilities, and better accuracy as k increases or R decreases, as both of these factors reduce τ_v relative to τ_{VE}. Figure 6b shows the influence of dilatational relaxation: when Λ approaches unity, the rapid compression of the solid phase causes the axial strain to pass through a maximum. That is, the rising pore pressure tends to expand the porous network, but this is offset by the contraction of the solid phase. The effect is exaggerated in these calculations, because we have set ψ_D equal to ψ, whereas it is expected to relax much more slowly. Nevertheless, Figure 7 shows that the dilatational relaxation improves the accuracy of the fit, particularly if eq. (29) is only applied to the data up to the peak in the strain. This calculation illustrates two points: first, if dilatational relaxation is rapid, it is revealed by the occurrence of a maximum in the strain recovery curve; second, even when this phenomenon occurs, accurate values can be obtained for the permeability by fitting the data before the maximum. None of the experimental curves from the preliminary study [20] exhibit a maximum, so we conclude (based on Figure 7) that the dilatational relaxation in cement paste is negligible, and the permeabilities extracted from the DP experiment are accurate within ~10%.

2.4. Unsaturated elastic materials

A much more serious problem than VE relaxation is the presence of air bubbles in the pore liquid, because the rise in pore pressure is delayed while the gas in the bubble is being compressed. Therefore, in this section we will revise the elastic analysis to allow for a volume fraction, v, of air in the pore liquid. Since we are concerned with entrapped air, it is reasonable to assume that it is uniformly distributed throughout the body. (The approach we will take would not be appropriate for a partially dried body, where the air-filled pores are concentrated near the outer surface. However, it should be valid for the uniformly distributed desaturation resulting from consumption of water by hydration of cement.) Consider a volume V containing volume V_L of liquid and V_G of an ideal gas, subjected to pressure p. The volume of gas varies as

$$\frac{V_G(p)}{V_G(p_0)} = \frac{p_0}{p} \tag{60}$$

and that of the liquid varies as

$$\frac{V_L(p) - V_L(p_0)}{V_L(p_0)} = -\frac{p - p_0}{K_L} \tag{61}$$

so the total volume is given by

$$V(p) = V_G(p_0)\left(\frac{p_0}{p}\right) + V_L(p_0)\left(1 - \frac{p - p_0}{K_L}\right) \tag{62}$$

If we define the apparent bulk modulus of the liquid / gas mixture to be K_L^A, then

$$\frac{1}{K_L^A} = -\frac{1}{V(p_0)}\frac{dV(p)}{dp} = \frac{1 - v}{K_L} + \frac{v p_0}{p^2} \tag{63}$$

where $v = V_G(p_0)/V(p_0)$ is the initial volume fraction of gas in the liquid. Figure 8 shows that K_L^A remains well below K_L, even when the pressure is 10 MPa, if $v \geq 0.01$. The amount of entrapped air in concrete is typically estimated to be ~3%, unless special precautions are taken, so the pore liquid can be expected to be much more compliant than in a fully saturated sample. We will evaluate this quantitatively by replacing K_L with K_L^A in the continuity equation, and calculating the effect on the strain.

To account for the presence of air, we replace K_L with K_L^A in eq. (8) of ref. 23; as a result, eq. (5) becomes

$$\frac{\dot{p}}{M_v} + b\dot{\varepsilon} + \frac{\phi v p_0 \dot{p}}{p^2} = \frac{k}{\eta_L}\nabla^2 p \tag{64}$$

where we redefine the Biot modulus as

$$\frac{1}{M_v} = \frac{\phi(1-v)}{K_L} + \frac{b-\phi}{K_S} \tag{65}$$

Consequently, the first term on the left side of eq. (11) is replaced by

$$\left(1+\frac{a}{p^2}\right)\frac{\partial p}{\partial \theta} \tag{66}$$

where

$$a = \frac{\lambda v \phi K_p p_0}{b\left[1-(1-\beta)b\lambda\right]} \tag{67}$$

As long as $a > 0$, the continuity equation is nonlinear and cannot be solved analytically. However, it can be solved numerically, as explained in Appendix 3.

Figure 9 shows the pressure distribution in a cylinder containing a negligible amount of entrapped air ($v = 10^{-4}$) and a typical quantity ($v = 0.03$), subjected to $p = 7$ MPa at time $\theta = 0$. In the former case, the pressure rises instantly to the applied pressure at the surface, $u = r/R = 1$; the interior rises smoothly to that pressure by the time $\theta = 1$. As shown in Figure 9b, when entrapped air is present, the internal pressure rises slowly. Once the pressure wave reaches the axis of the cylinder ($u = 0$), when $\theta \approx 2$, the interior pressure equilibrates rapidly, but the whole process takes about three times as long as for a saturated sample.

Figure 10 provides a comparison of the strain evolution for samples of cement paste with the properties cited earlier, containing entrapped air at volume fractions of $v = 0$, 0.01, 0.02, and 0.03. The time to equilibrate the strain doubles by the addition of 1% air and triples with 3%. At such high air contents there is an inflection in the curve that alerts the experimentalist to the problem, but to avoid errors it is advisable to perform a series of pressurization/depressurization cycles to insure that they are identical. If air is present, it will dissolve gradually, so that the curves will converge toward a constant shape from which the permeability can be extracted with confidence. To avoid errors from entrapped air, the simulations indicate that v must be held below 0.1%, which is quite low for cementitious materials. For $v > 0.001$, the initial strain is found to obey eq. (26), indicating that the liquid/gas mixture is too compliant (compared to K_p) to contribute to the rigidity of the sample. It would be necessary to mix under vacuum to achieve such low gas contents; alternatively, it might be useful to mix under a flow of carbon dioxide, as that gas is so soluble that it will be rapidly eliminated by pressurization.

3. Discussion

Dynamic pressurization permits measurement of the permeability of materials as delicate as aerogels [19] and as rigid as cement paste [20]. In the present paper, we have provided an analysis that permits calculation of the bulk moduli of the porous network (K_p) and the solid phase (K_S), as well as the permeability (k). The accuracy of the calculations, particularly for K_S, can be compromised by viscoelastic effects, but for cementitious materials the errors are expected to be small ($< 10\%$ for k). If significant VE relaxation occurs, it is reflected as a maximum in the strain recovery curve. More problematic is the effect of entrapped air, which may be difficult to avoid. Precautions should be taken to minimize entrapped air during sample preparation, but it is always advisable to use a sequence of pressurization/depressurization steps to insure that the relaxation curves are identical. In that way, the results are certain to be free of error caused by gas pockets.

It is important to avoid damaging the sample during depressurization. A sudden drop of pressure causes tensile stress equal to about half the pressure drop. For a brittle material, this may cause microcracking that raises the permeability. To avoid damage, one can either use pressure jumps that are small compared to the tensile strength, or use a large compressive jump followed by a slow release of pressure. If the pressure is released over a period equal to the hydrodynamic relaxation time of the sample, the tensile stress is reduced by an order of magnitude compared to that produced by a sudden depressurization.

Experimental tests of the method are presented in a companion paper [32].

Acknowledgments

This work was supported by a grant from the National Science Foundation, Division of Civil and Mechanical Systems, grant CMS-0070092.

Appendix 1. Solution of eq. (11)

The solution proceeds in much the same way as in ref. 9. First we apply the Laplace transform with respect to θ [30],

$$\mathcal{L}\left[y(u,\theta)\right] = \tilde{y}(u,s) = \int_0^\infty e^{-s\theta}\, y(u,\theta)\, d\theta \tag{68}$$

where s is called the transform parameter. This reduces the continuity equation to an ordinary differential equation in u that is easily solved. The transformed pressure is given as a function of p_A and the volume-averaged pressure, $\langle\tilde{p}(s)\rangle$; the latter quantity is found by averaging the solution over u, solving for the average pressure, and substituting that into the solution for $\tilde{p}(u,s)$. The result is

$$\tilde{p}(u,s) = \tilde{p}_A(s)\left\{1 - \frac{(1-\lambda)\left[1-g(u,s)\right]}{1-(1-\beta)b\lambda h(s)}\right\} \tag{69}$$

where

$$g(u,s) = \frac{I_0\left(u\sqrt{s}\right)}{I_0\left(\sqrt{s}\right)} \tag{70}$$

and

$$h(s) = \langle g(u,s)\rangle = \frac{2I_1\left(\sqrt{s}\right)}{\sqrt{s}\, I_0\left(\sqrt{s}\right)} \tag{71}$$

The average pore pressure is found by averaging eq. (69), then the transformed strain is found from the transform of eq. (15):

$$\tilde{\varepsilon}_z = \frac{\tilde{b}\langle\tilde{p}(s)\rangle - \tilde{p}_A}{3K_p} \tag{72}$$

The result is

$$\tilde{\varepsilon}_z = \left(\frac{b-1}{3K_p}\right)\mathcal{L}\left[p_A\right] - \frac{b(1-\lambda)}{3K_p}\,\tilde{\Omega}(s)\,\mathcal{L}\left[\frac{dp_A}{d\theta}\right] \tag{73}$$

where

$$\tilde{\Omega}(s) = \frac{1-h(s)}{s\left[1-(1-\beta)b\lambda h(s)\right]} \tag{74}$$

Numerical inversion of this equation is discussed in Appendix 2. We can, however, examine its early time behavior analytically. Expanding eq. (74) in a Taylor series yields

$$\tilde{\Omega}(s) \approx \frac{1}{s} - \frac{2\left[1-(1-\beta)b\lambda\right]}{s^{3/2}} + \cdots \tag{75}$$

Large values of s correspond to small values of time, so the early behavior of Ω is found by neglecting terms involving reciprocals of higher powers of s in eq. (75). The result is eq. (19).

The strain following a step increase in pressure is obtained by setting $\tilde{p}_A$ equal to p_A/s. For the case where the pressure jumps to p_A at $\theta = 0$, then steps back to zero at $\theta = \theta_d$, the transform of the pressure is

$$\tilde{p}_A = \int_0^{\theta_d} e^{-s\theta}\, p_A(\theta)\, d\theta = \left(\frac{p_A}{s}\right)\left(1 - e^{-s\theta_d}\right) \tag{76}$$

The transform of $dp_A/d\theta$ is $s\,\tilde{p}_A$; substituting these results into eq. (73) and inverting the transform leads to eq. (27).

If the pressure in the chamber is reduced linearly, according to eq. (41), the Laplace transform of the pressure at the exterior surface of the sample is

$$\tilde{p}_{ext} = \left(\frac{p_A}{s}\right)\left\{1 + \frac{1}{s\theta_0}\left[\left(1 - e^{-s\theta_d}\right) - \left(1 - e^{-s(\theta_d+\theta_0)}\right)\right]\right\} \tag{77}$$

From eq. (73), we obtain

$$3K_p\,\tilde{\varepsilon}_z = -(1-b)\,\tilde{p}_{ext} - b(1-\lambda)\,\tilde{\Omega}(s)\,s\,\tilde{p}_{ext} \tag{78}$$

Inserting eq. (77) into eq. (78) and inverting the transform yields eq. (42) of the text.

Appendix 2. Numerical evaluation of Ω

The inversion of the function $h(s)$ can be done analytically, as explained in ref. 19, but evaluation of $\tilde{\Omega}$ must be done numerically. We used the Stehfest algorithm in the routine NumericalInversion [33] in *Mathematica*® [34]. The notebook with the detailed calculations is available from the present author. Values of $\tilde{\Omega}$ were generated at equal logarithmic intervals in time over $10^{-4} \leq \theta \leq 3$, and the data were fitted to eq. (17) using *KaleidaGraph*® [35].

Appendix 3. Numerical solution of eq. (64)

The numerical solution of the continuity equation for a body whose pores contain gas pockets in the liquid,

$$\left(1+\frac{a}{p^2}\right)\frac{\partial p}{\partial \theta}+\left(\frac{(1-\beta)b\lambda}{1-(1-\beta)b\lambda}\right)\frac{\partial \langle p\rangle}{\partial \theta}-\left(\frac{\lambda}{1-(1-\beta)b\lambda}\right)\frac{\partial p_A}{\partial \theta}=\frac{1}{u}\frac{\partial}{\partial u}\left(u\frac{\partial p}{\partial u}\right) \tag{79}$$

was obtained using the function NDSolve in *Mathematica*® [34]. The routine cannot accept boundary or initial conditions at zero, so the initial conditions were specified at $\theta =$ 10^{-10} and the symmetry condition, $\partial p/\partial u|_{u=0} = 0$, was applied at $u = 10^{-10}$. To avoid a discontinuity in the boundary condition, the pressure jump was written as

$$p(1,\theta) = p_0 + (p_A - p_0)\tanh\left(10^4\,\theta\right) \tag{80}$$

The term involving the derivative of p_A in eq. (79) was also written as the derivative of the tanh function. The term involving the derivative of the average pressure was written as the integral of the derivative of p. The maximum step size for u and θ was set to 10^{-3}, which was sufficient to eliminate messages indicating failure to converge. When the volume fraction of air was set to a value $\leq 10^{-3}$, the numerical solution converged on the analytical solution for the air-free case. The solution is returned as an interpolating function, which can be used to plot or list the pressure, or integrated to get the average pressure and then used to find the strain from eq. (15). The pressure distributions in Figure 9 were produced from the interpolating function using the *Mathematica*® plotting function, Plot3D.

References

---

1. C. Hall and W.D. Hoff, *Water transport in brick, stone and concrete* (Spon Press, London, 2002)

2. G.W. Scherer, “Stress from crystallization of salt”, Cement Concr. Res. 34 (2004) 1613-1624

3. T.C. Powers, L.E. Copeland, and H. M. Mann, “Capillary Continuity or Discontinuity in Cement Pastes,” *Journal of the Portland Cement Association Research and Development Laboratory*, May (1959) 38-48

4. R.D. Hooton and A.S. El-Dieb, "Evaluation of water permeability of high performance concrete", Concrete Under Severe Conditions, Vol. 1, ed. K. Sakai, N. Banthia, O.E. Gjørv (1995) pp. 423-432

5. G.W. Scherer, “Measuring Permeability of Rigid Materials by a Beam-Bending Method: I. Theory”, J. Am. Ceram. Soc. 83 [9] (2000) 2231-2239; Erratum, J. Am. Ceram. Soc. 87 [8] (2004) 1612-1613

6. W. Vichit-Vadakan and G.W. Scherer, “Measuring Permeability of Rigid Materials by a Beam-Bending Method: III. Cement Paste”, J. Am. Ceram. Soc. **85** [6] 1537–44 (2002) ; Erratum, J. Am. Ceram. Soc. **87** [8] (2004) 1615

7. W. Vichit-Vadakan and G.W. Scherer, “Measuring permeability and stress relaxation of young cement paste by beam-bending”, Cement Concrete Res. **33** (2003) 1925-1932

8. J.J. Valenza II and G.W. Scherer, “Measuring Permeability of Rigid Materials by a Beam-Bending Method: V. Isotropic Rectangular Plates of Cement Paste”, J. Am. Ceram. Soc. **87** [10] (2004) 1927-1931

9. G.W. Scherer, “Thermal expansion kinetics: Method to measure permeability of cementitious materials: I, Theory”, J. Am. Ceram. Soc. 83 [11] (2000) 2753-61; Erratum, J. Am. Ceram. Soc. 87 [8] (2004) 1609-1610

10. H. Ai, J.F. Young, and G.W. Scherer, “Thermal expansion kinetics: Method to measure permeability of cementitious materials: II, Application to hardened cement paste”, J. Am. Ceram. Soc. 84 [2] (2001) 385-391; Erratum, J. Am. Ceram. Soc. 87 [8] (2004) 1611

11. J.J. Valenza and G.W. Scherer, “Evidence of anomalous thermal expansion of water in cement paste”, Cement Concr. Res. **35** (2005) 57-66

12. J.P. Ciardullo, D.J. Sweeney, and G.W. Scherer, “Thermal expansion kinetics: Method to measure permeability of cementitious materials: IV, Effect of thermal gradients”, J. Am. Ceram. Soc. **88** [5] (2005) 1213–1221

13. G.W. Scherer, H. Hdach, and J. Phalippou, “Thermal Expansion of Gels: A Novel Method for Measuring Permeability”, J. Non-Cryst. Solids, 130 (1991) 157-170; errata, J.

Non-Cryst. Solids 194 (1996) 326

14. S.L. Meyers, "Thermal expansion characteristics of hardened cement paste and of concrete", Proc. Highway Res. Board 30 (1950) 193-203

15. R.A. Helmuth, "Dimensional changes of hardened Portland cement pastes caused by temperature changes", Proc. Highway Res. Board 40 (1961) 315-335

16. Z.P. Bazant, "Delayed thermal dilatations of cement paste and conrcete due to mass transport", Nuclear Eng. Design 14 (1970) 308-318

17. G.C. Simmons, "Thermopermeametry of Sand Mortars", Senior thesis, Dept. Civil & Env. Eng., Princeton University, 2005

18. G.W. Scherer, J.J. Valenza II, and G.C. Simmons, "New methods to measure permeability in porous materials", submitted to Cement & Concrete Research

19. J. Gross and G.W. Scherer, "Dynamic Pressurization: Novel method for measuring fluid permeability", J. Non-Cryst. Solids 325 (2003) 34-47

20. Z.C. Grasley, J.J. Valenza II, G.W. Scherer, D.A. Lange, "Measuring permeability and bulk modulus of cementitious materials", to be published in the proceedings of Concreep7, Int. Conf. Creep, Shrinkage and Durability of Concrete and Concrete Structures, Nantes, 12-14 Sept. 2005

21. M.A. Biot, "Theory of elasticity and consolidation for a porous anisotropic solid", J. Appl. Phys. 26 [2] (1955) 182-185

22. O. Coussy, *Mechanics of Porous Continua* (Wiley, New York, 1995)

23. G.W. Scherer, "Characterization of Saturated Porous Bodies", Concr. Sci. Eng. 37 [265] (2004) 21-30

24. J. Happel and H. Brenner, *Low Reynolds number hydrodynamics* (Martinus Nijhoff, Dordrecht, 1986)

25. G.W. Scherer, "Stress in Aerogel during Depressurization of Autoclave: I. Theory", J. Sol-Gel Sci. Tech. 3 (1994) 127-139

26. D. R. Lide (ed.), *Handbook of Chemistry and Physics.* (CRC Press, New York, 1997)

27. S. Mindess and J. F. Young, *Concrete* (Prentice-Hall, Englewood Cliffs, NJ, 1981) p. 481

28. G.W. Scherer, *Relaxation in Glass and Composites* (Wiley, New York, 1986; reprinted by Krieger, Malabar, FL, 1992) Ch. 7

29. R.S. Lakes, "Foam structures with a negative Poisson's ratio", Science 235 (1987) 1038-1040

30. F.B. Hildebrand, *Advanced Calculus for Applications* (Prentice-Hall, Englewood Cliffs, New Jersey, 1962)

---

31. G.W. Scherer, “Thermal expansion kinetics: Method to measure permeability of cementitious materials: III, Effect of viscoelasticity”, J. Am. Ceram. Soc. 87 [8] (2004) 1509-1516

32. Z.C. Grasley, J.J. Valenza II, G.W. Scherer, D.A. Lange, “Dynamic Pressurization Method for Measuring Permeability and Modulus: II. Experimental Study of Cement Paste”, to be submitted to

33. Arnaud Mallet, University of Mauritius (Copyright © 2000)

34. Wolfram Research, Inc., 100 Trade Center Drive, Champaign, IL, 61820-7237, USA.

35. Synergy Software, 2457 Perkiomen Avenue, Reading, PA 19606 USA

Figure Captions

Figure 1. Schematic of dynamic pressurization experiment. The sample is enclosed in a vessel full of fluid. Initially, the pressure in the vessel (p_v) and in the pore fluid (p_p) is equal to atmospheric pressure (p_0). At the start of the experiment (time $t = 0^+$), the pressure in the vessel is suddenly raised to some higher value, p_A; the sample is compressed by a linear strain equal to ε_0, so the pore pressure rises, but does not immediately reach p_A. Over time, the liquid from the vessel penetrates the pores of the sample until the pore pressure equilibrates at p_A; the final strain (ε_∞) results from compression of the solid phase by the applied pressure.

Figure 2. Approximation of the hydrodynamic relaxation function, $\Omega(\theta)$, using eq. (17); symbols represent the value of the function (evaluated using the methods described in Appendix 2) and the solid curve is the approximation. The function is evaluated using parameter values typical of concrete: $\beta = 1/2$, $b = 2/3$, $\lambda = ¼$.

Figure 3. Schematic of strain produced during pressurization (at time $t/\tau_v = 0$), followed by depressurization (at time $t/\tau_v = 1$). In this case, before the pressure is released, the pore pressure has very nearly equilibrated at p_A, so the shapes of relaxation curves are identical.

Figure 4. Normalized stress during step pressurization over a period equal to $\theta_d = 1$, followed by depressurization at a linear rate over reduced time interval θ_0.

Figure 5. Normalized peak stress during depressurization at a linear rate as a function of the depressurization interval, *θ0.*

Figure 6. Calculated axial strain, normalized by $-\varepsilon_\infty = p_A/3K_S$, for various values of $\Lambda = \tau_v/\tau_{VE}$; symbols are values obtained by numerical evaluation of eq. (56) and curves are fits to eq. (20). In (a) no dilatational relaxation occurs ($\mu = 1$), but in (b) the bulk modulus of the solid relaxes to 0.3 times its original value; in the latter case, only data up to the peak in the strain are used in the fit when $\Lambda = 1$.

Figure 7. Results of fitting eq. (20) to values obtained from numerical evaluation of eq. (56) for various values of $\Lambda = \tau_v/\tau_{VE}$, where "$\tau_v$ input" was used in the evaluation and

"τ_v fit" was obtained from the fit; perfect agreement is represented by the horizontal dashed line at a ratio of unity. The upper curve is for a material in which there is no dilatation of the solid phase ($\mu = 1$) and the lower curve applies when the bulk modulus of the solid relaxes to 0.3 times its instantaneous value ($\mu = 0.3$). The curves are for fits to all data up to $t = \tau_v$, but the square symbols are for fits up to the peak in the strain curve (see Figure 6b).

Figure 8. Ratio of apparent bulk modulus of gas/liquid mixture, K_L^A, to true bulk modulus of liquid, K_L, for several values of the volume fraction of air, v, as a function of the applied pressure, p. The calculation assumes $K_L = 2.2$ GPa (characteristic of water) and $p_0 = 0.1$ MPa (atmospheric pressure).

Figure 9. Pressure distribution as a function of radial position, $u = r/R$, and time, $\theta = t/\tau_v$ for volume fractions of air equal to (a) $v = 0.0001$ and (b) $v = 0.03$.

Figure 10. Axial strain, ε_z, as a function of time, $\theta = t/\tau_v$ for volume fractions of air (for curves from left to right) equal to $v = 0, 0.01, 0.02, 0.03$.

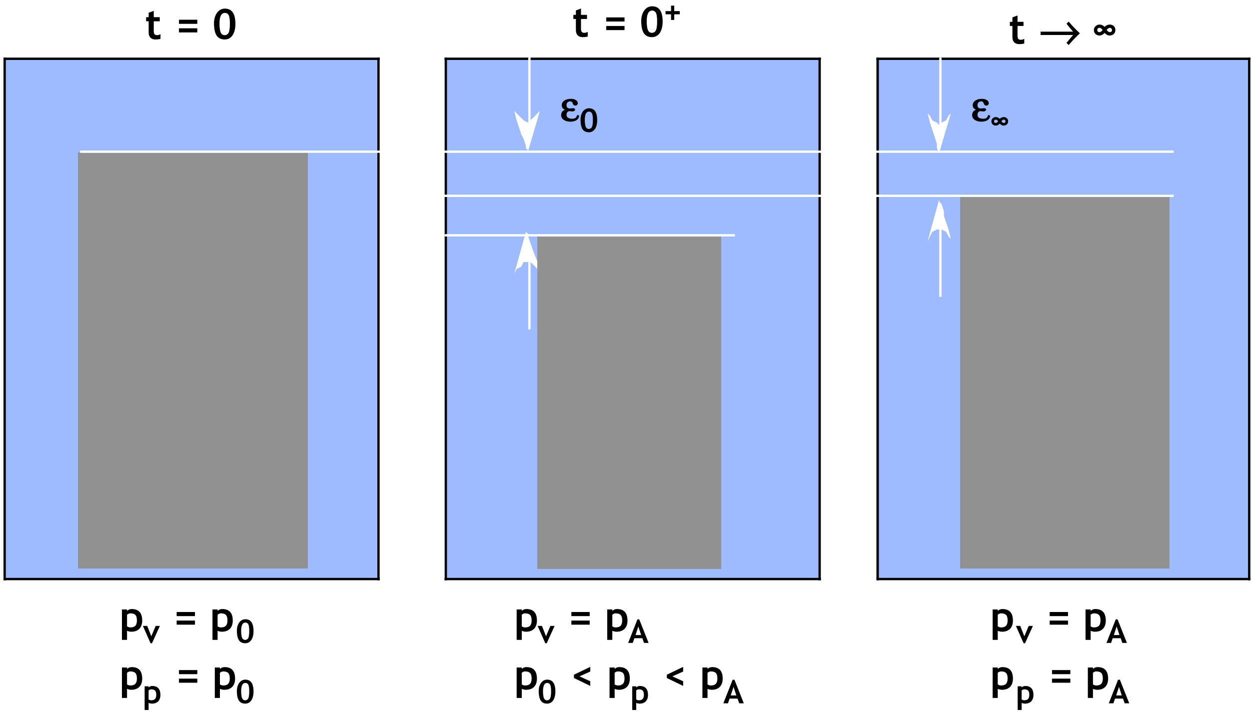

Figure 1. Schematic of dynamic pressurization experiment. The sample is enclosed in a vessel full of fluid. Initially, the pressure in the vessel (p_v) and in the pore fluid (p_p) is equal to atmospheric pressure (p_0). At the start of the experiment (time $t= 0^+$), the pressure in the vessel is suddenly raised to some higher value, p_A; the sample is compressed by a linear strain equal to ε_0, so the pore pressure rises, but does not immediately reach p_A. Over time, the liquid from the vessel penetrates the pores of the sample until the pore pressure equilibrates at p_A; the final strain (ε_∞) results from compression of the solid phase by the applied pressure.

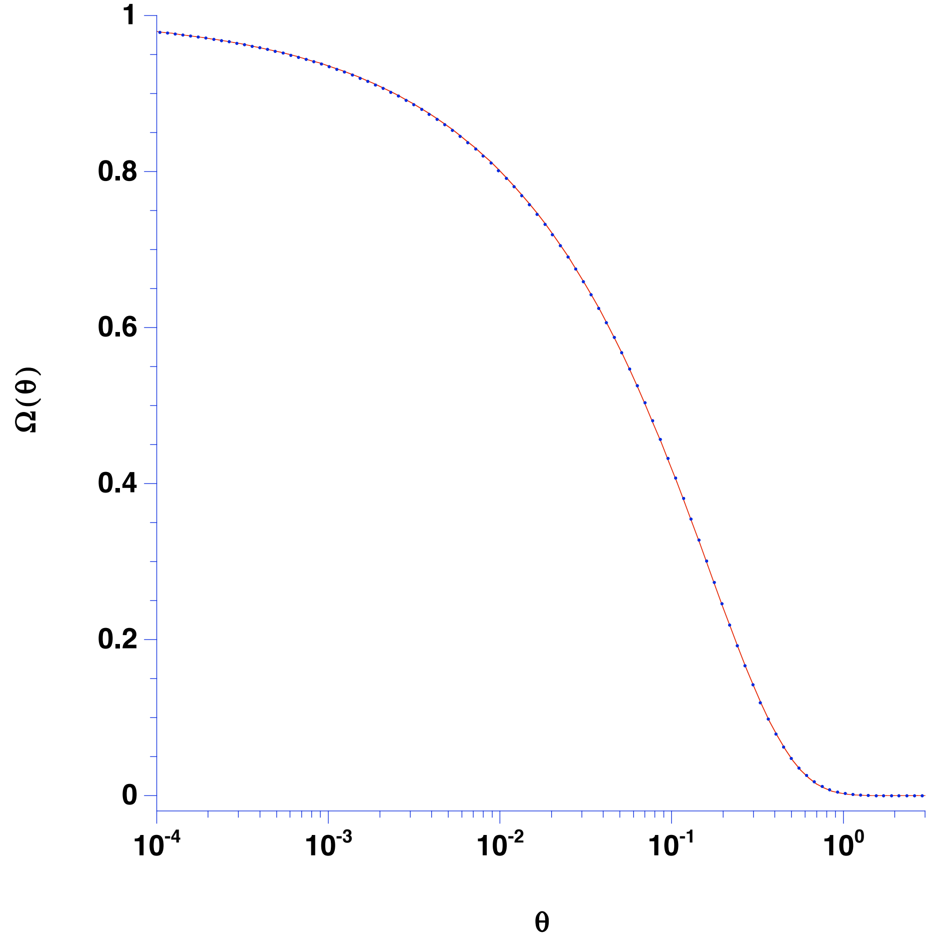

Figure 2. Approximation of the hydrodynamic relaxation function, $\Omega(\theta)$, using eq. **(17)**; symbols represent the value of the function (evaluated using the methods described in Appendix 2) and the solid curve is the approximation. The function is evaluated using parameter values typical of concrete: $\beta = 1/2$, $b = 2/3$, $\lambda = ¼$.

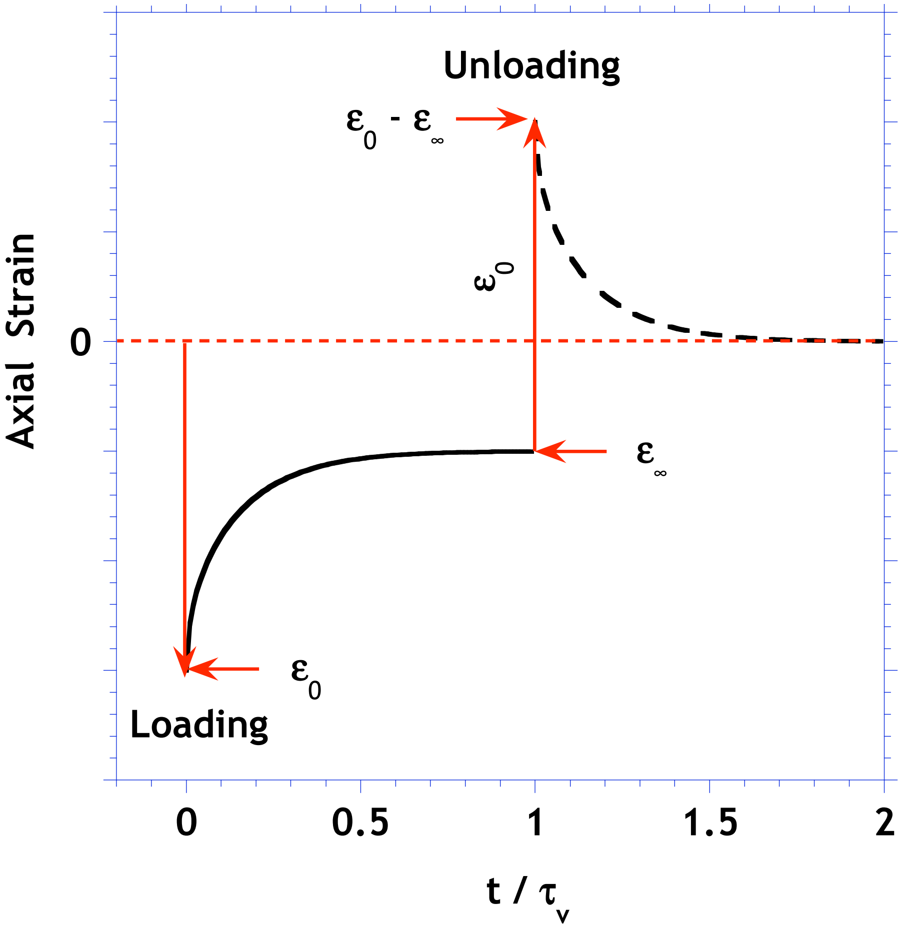

Figure 3. Schematic of strain produced during pressurization (at time $t / \tau_v = 0$), followed by depressurization (at time $t / \tau_v = 1$). In this case, before the pressure is released, the pore pressure has very nearly equilibrated at p_A, so the shapes of relaxation curves are identical.

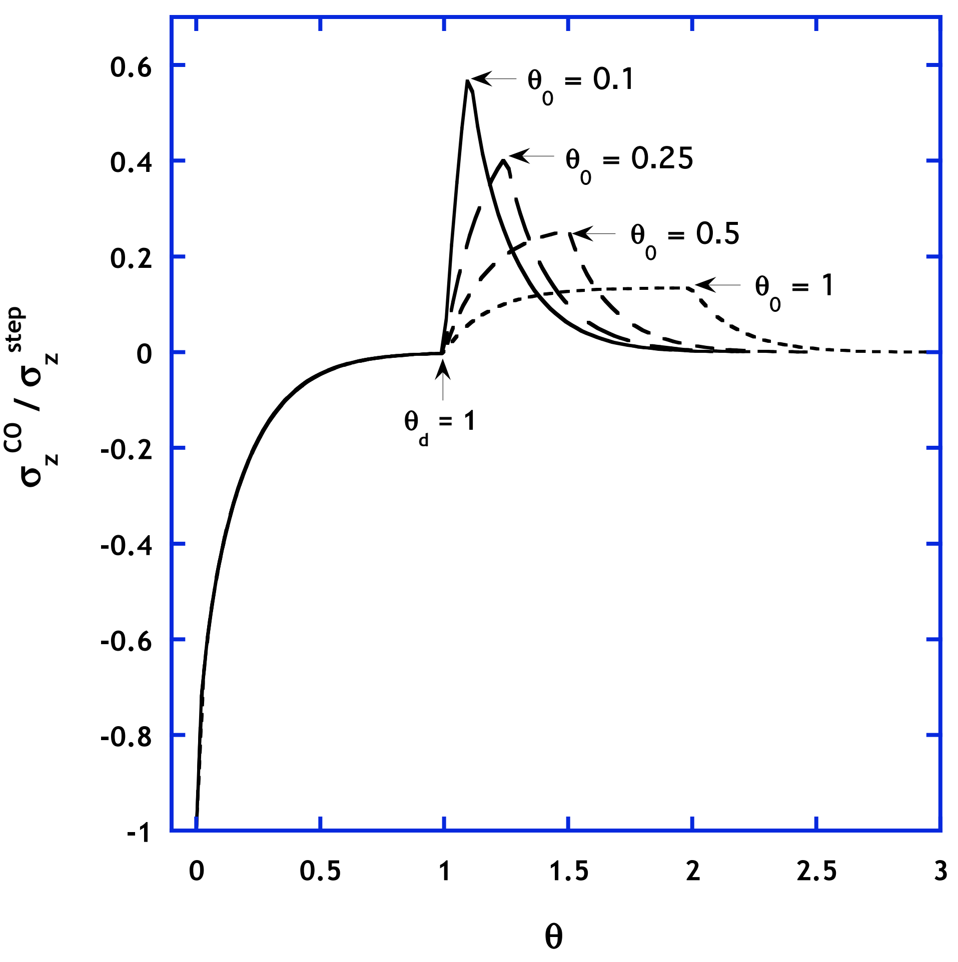

Figure 4. Normalized stress during step pressurization over a period equal to $\theta_d = 1$, followed by depressurization at a linear rate over reduced time interval θ_0.

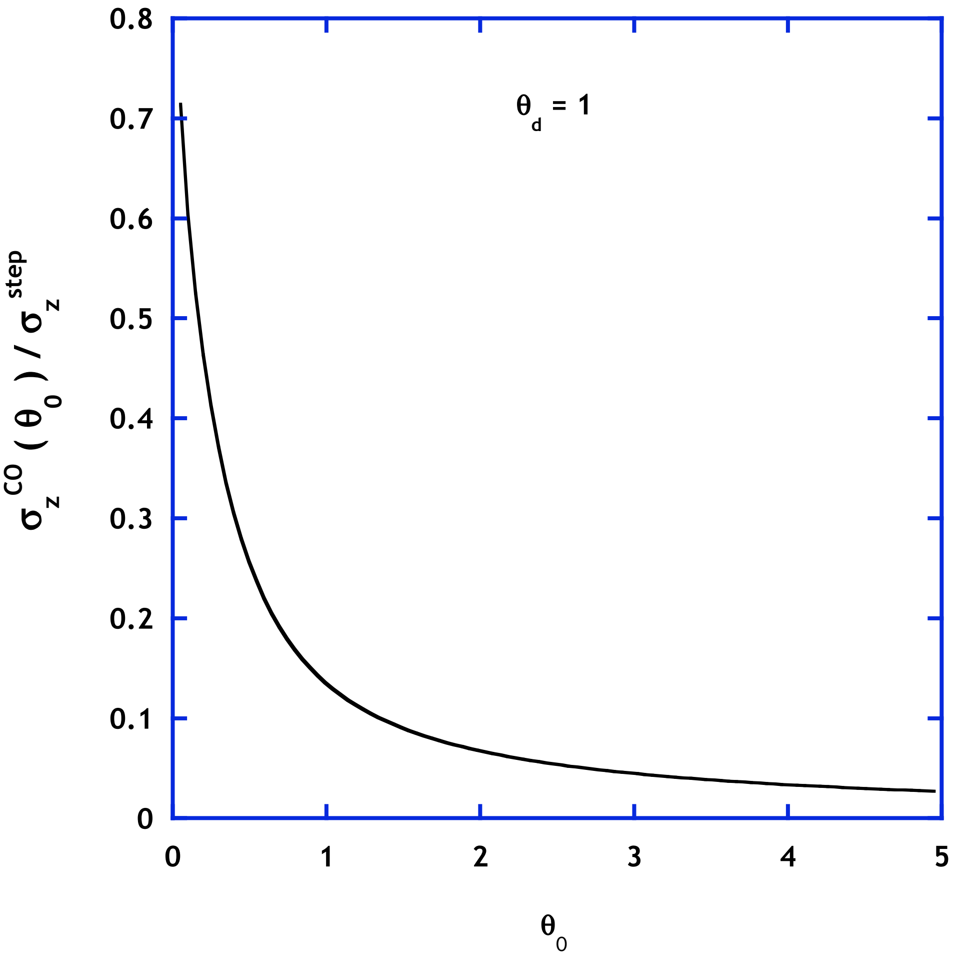

Figure 5. Normalized peak stress during depressurization at a linear rate as a function of the depressurization interval, θ_0.

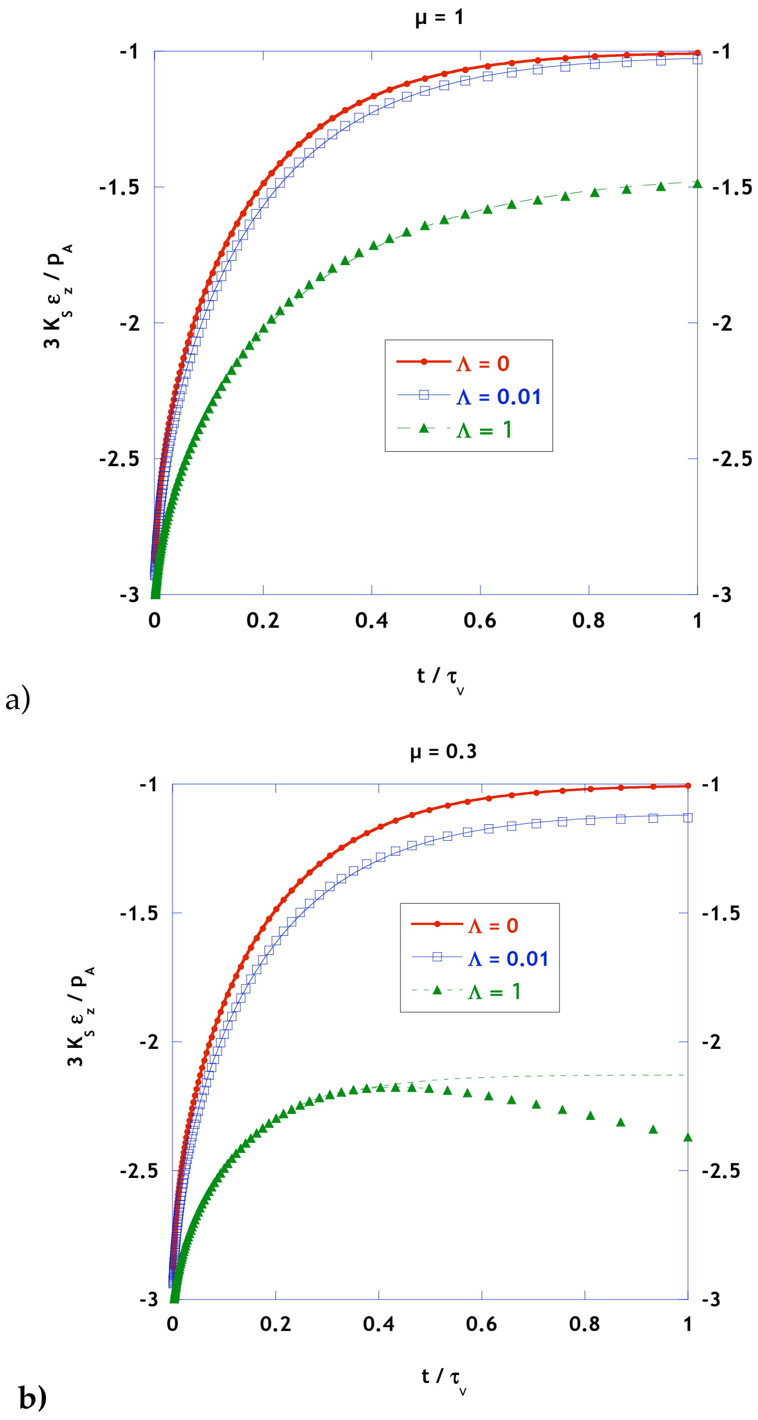

Figure 6. Calculated axial strain, normalized by $-\varepsilon_\infty = p_A / 3K_S$, for various values of $\Lambda = \tau_v / \tau_{VE}$; symbols are values obtained by numerical evaluation of eq. (56) and curves are fits to eq. (20). In (a) no dilatational relaxation occurs (μ = 1), but in (b) the bulk modulus of the solid relaxes to 0.3 times its original value; in the latter case, only data up to the peak in the strain are used in the fit when $\Lambda = 1$.

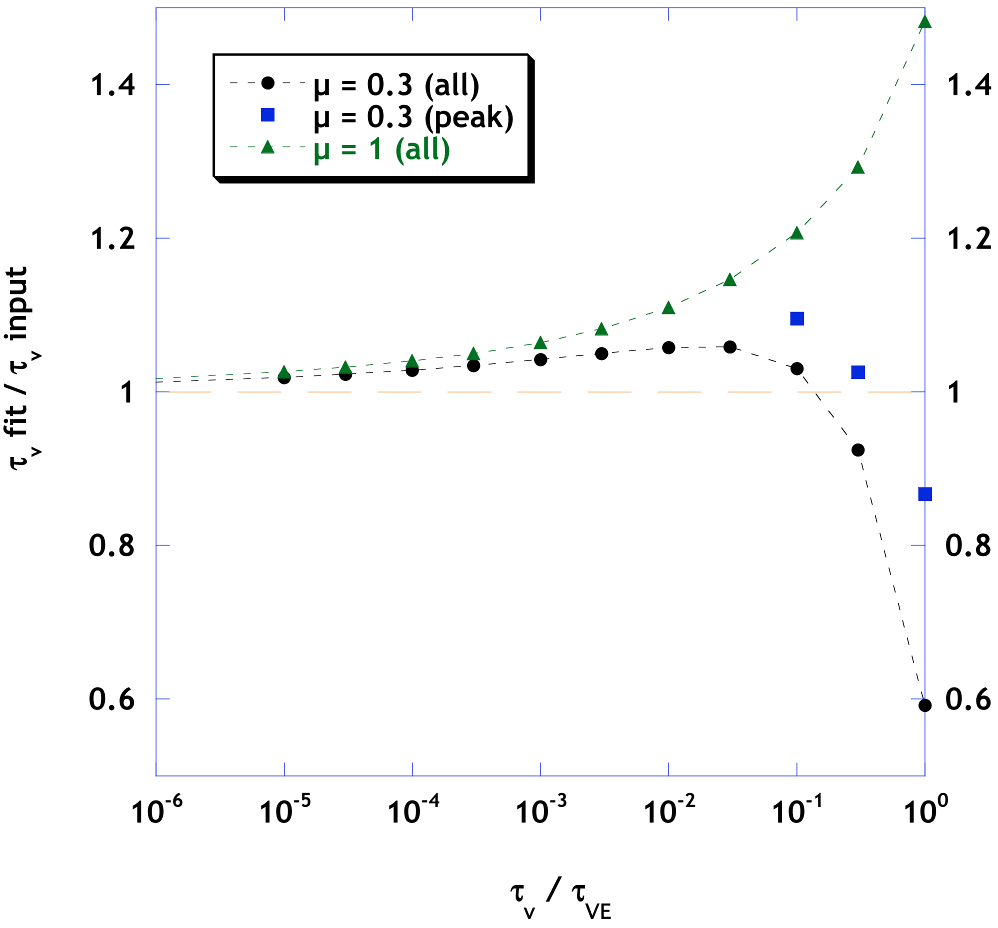

Figure 7. Results of fitting eq. (20) to values obtained from numerical evaluation of eq. (56) for various values of $\Lambda = \tau_v / \tau_{VE}$, where "$\tau_v$ input" was used in the evaluation and "τ_v fit" was obtained from the fit; perfect agreement is represented by the horizontal dashed line at a ratio of unity. The upper curve is for a material in which there is no dilatation of the solid phase ($\mu = 1$) and the lower curve applies when the bulk modulus of the solid relaxes to 0.3 times its instantaneous value ($\mu = 0.3$). The curves are for fits to all data up to $t = \tau_v$, but the square symbols are for fits up to the peak in the strain curve (see Figure 6b).

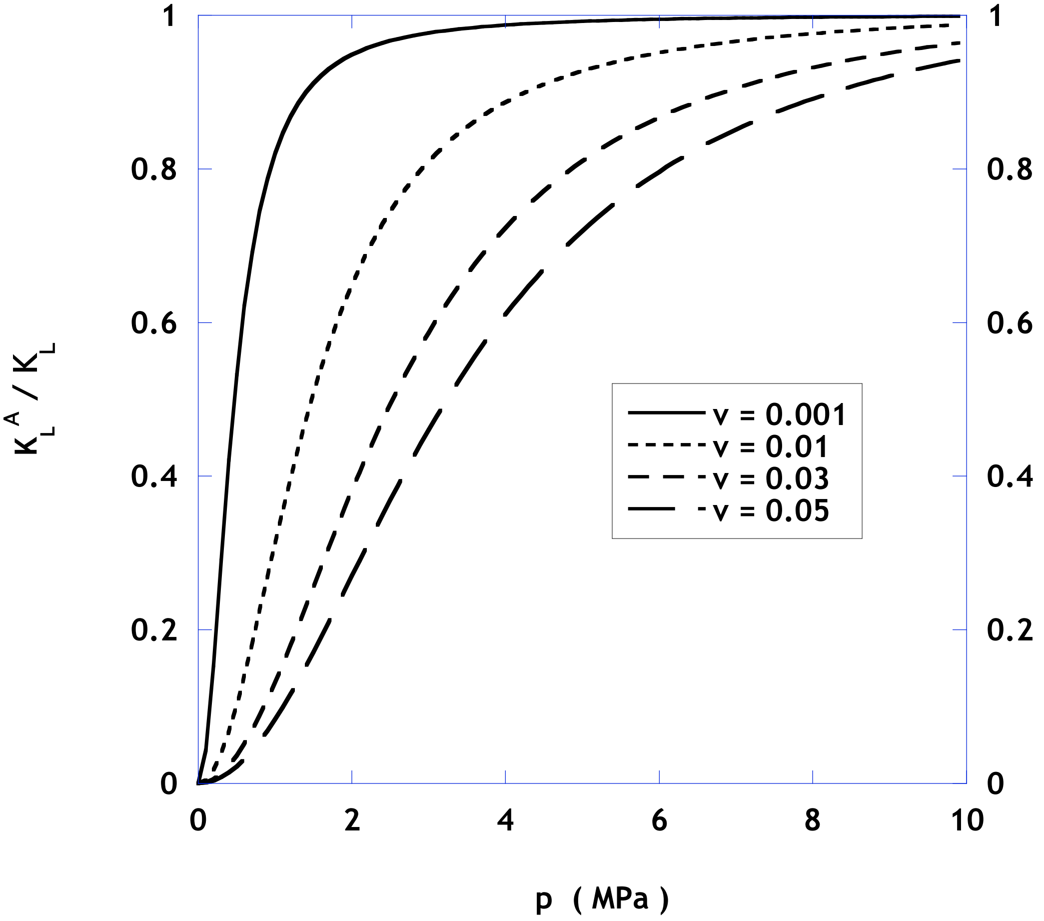

Figure 8. Ratio of apparent bulk modulus of gas/liquid mixture, K_L^A, to true bulk modulus of liquid, K_L, for several values of the volume fraction of air, v, as a function of the applied pressure, p. The calculation assumes $K_L = 2.2$ GPa (characteristic of water) and $p_0 = 0.1$ MPa (atmospheric pressure).

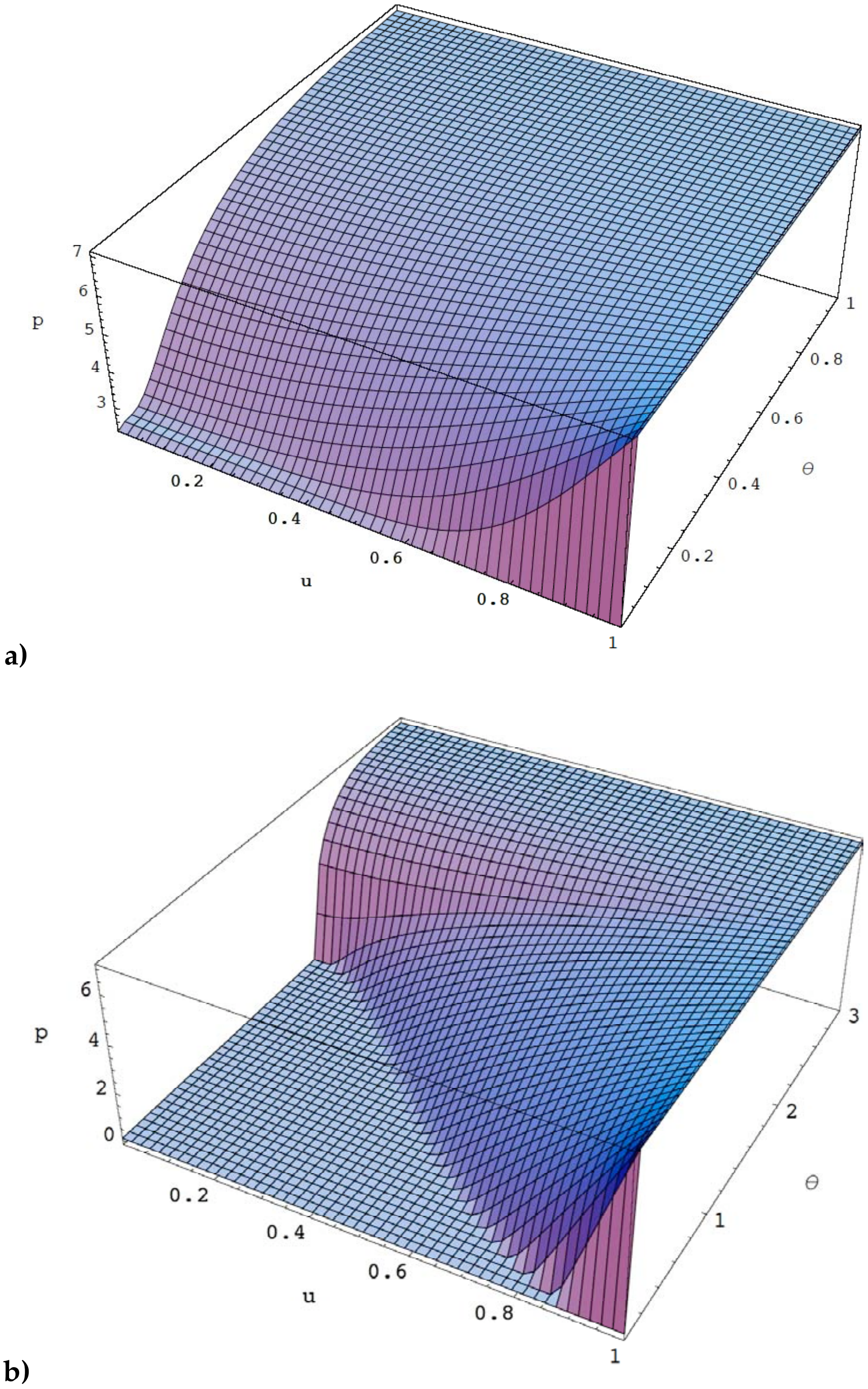

Figure 9. Pressure distribution as a function of radial position, $u = r/R$, and time, $\theta = t/\tau_v$ for volume fractions of air equal to (a) $v = 0.0001$ and (b) $v = 0.03$.

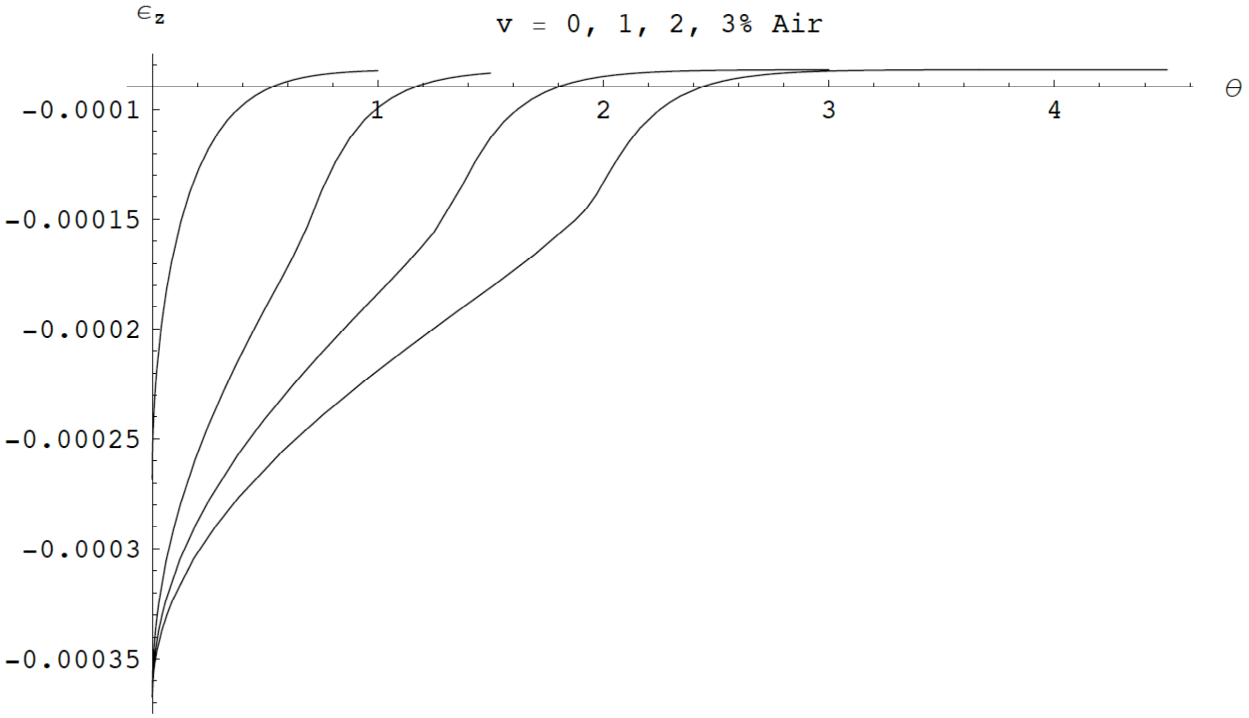

Figure 10. Axial strain, ε_z, as a function of time, $\theta = t / \tau_v$ for volume fractions of air (for curves from left to right) equal to $v = 0, 0.01, 0.02, 0.03$.